Journal of Metals, Materials and Minerals, 34(4), 1964, 2024

Nanostructure of TiO_2 and WO_3 multilayer films deposited on ITO glass for electrochromic enhanced photocatalytic activity

Atsakorn CHUENKRUIT[1], Watcharaporn THONGJOON[1], Kamon AIEMPANAKIT[1], Montri AIEMPANAKIT[2], and Chantana AIEMPANAKIT[3,*]

[1] *Department of Physics, Faculty of Science and Technology, Thammasat University, Pathumthani, 12121, Thailand*
[2] *Department of Physics, Faculty of Science, Silpakorn University, Nakhon Pathom, 73000, Thailand*
[3] *Division of Physics, Faculty of Science and Technology, Rajamangala University of Technology Thanyaburi, Pathumthani, 12110, Thailand*

***Corresponding author e-mail**: chantana_e@rmutt.ac.th

Received date:
17 February 2024
Revised date:
30 July 2024
Accepted date:
24 August 2024

Keywords:
Oblique angle deposition;
TiO_2;
WO_3;
Electrochromic;
Photocatalytic

Abstract

The photocatalytic activity (PA) by electrochromic (EC) enhancement of single and multilayer films of TiO_2, WO_3, TiO_2/WO_3, and WO_3/TiO_2 was investigated. All films were deposited from metal on an ITO glass substrate using direct current (DC) magnetron sputtering via an oblique angle deposition (OAD) technique at 85°. Subsequently, a thermal oxidation (TO) process at 500°C was applied for the samples to form metal oxide films. The morphology, elemental composition, crystal structure, and optical properties were studied by using field emission scanning electron microscopy (FE-SEM), energy-dispersive X-ray spectroscopy (EDS), X-ray diffractometry (XRD), and UV-vis spectroscopy, respectively. The photocatalytic properties were investigated by showing the degradation rate of methylene blue (MB) solution as an organic pollutant that was examined under ultraviolet irradiation of 300 $\mu W \cdot cm^{-2}$. The film samples were investigated by comparing the pre-color and colored states that were achieved through the EC process. The EC properties of WO_3 led to increased charge insertion on the film surface. This observation was further supported by cyclic voltammetry (CV) testing, which revealed a higher current density for the thin film samples. The photodegradation results showed that the samples in the colored state exhibited a significantly higher degradation rate of MB compared to the pre-color state.

1. Introduction

In the past few years, titanium dioxide (TiO_2) nanostructures have gained popularity in a variety of applications, including sensors, self-cleaning, and the degradation of organic pollutants [1]. TiO_2 is widely recognized as an effective photocatalyst, especially at UV and NIR range. It was chosen as the preferred catalyst for photodegradation applications over other metal oxides. However, the photocatalytic efficiency of TiO_2 is limited by its band gap (E_g) of approximately 3.0 eV to 3.2 eV, but there are several ways to enhance this efficiency, including reducing e^--hole recombination [2], increasing e^--hole pair generation, and increasing charge separation and surface area [3]. The most common method for improving performance is to combine TiO_2 with other metal nanoparticles and coat them on top of TiO_2 [4,5]. However, this may reduce the active surface area between TiO_2 and the liquid pollutants, resulting in a decrease in catalyst efficiency. To address this problem, modifying TiO_2 with tungsten trioxide (WO_3) improves the charge separation efficiency, as WO_3 has a band gap of approximately 2.8 eV and a similar conduction band level to TiO_2 [6]. The primary function of WO_3 is to give and receive charges from the TiO_2 band and maintain them in an excited state for a certain period to reduce the recombination rate, also known as a heterojunction [7-9]. Furthermore, WO_3 is used in a variety of technological applications including EC devices and smart windows [10-12]. The electrochemical coloration is combined with intercalation of lighter ions such as H^+, Li^+, Na^+, and K^+ [13,14], which can increase the charge density on the film surface [15,16] and is related to the oxidation-reduction rate of degrading organic pollutants.

In this study, the two materials, Ti and W, were deposited on an indium-doped tin oxide (ITO) substrate with a nanorod structure to allow the multiple layers to synergistically increase the surface area, using the DC magnetron sputtering technique combined with OAD to increase the surface area of the films beyond that which dense film can achieve [17,18]. During the deposition process, the particles form an aligned nanorod array on the surface, which causes the shadowing effect. In addition, the deposition rate has a direct impact on film nucleation and growth. A higher deposition rate would cause adatoms on the surface to form an ordered alignment [19]. In this study, we intend to form the Ti thin film layer at a high deposition rate to achieve higher crystallinity with fewer defects, which is beneficial for minimizing the recombination of photogenerated e- and holes [20]. Furthermore, we aim to achieve a W thin film layer at a low deposition rate to create a porous structure, which improves EC performance by allowing e^- and cations to pass through more easily [21-26]. Furthermore, the TO technique was used to create metal oxide films of TiO_2 and WO_3 on an ITO glass substrate. External heat is used to create reactions inside

an open pipe, such as $Ti^{4+} + 2O^{2-} \rightarrow TiO_2$ and $W^{6+} + 3O^{2-} \rightarrow WO_3$. We demonstrated and compared the photocatalytic performance of 1-layer and 2-layer samples in their pre-colored and colored states by monitoring the degradation rate of MB solution under UV irradiance. The colored state, achieved through the EC process, involves the injection of e^- and cations into the film's structure (see Figure 1) [27]. This results in a high carrier density on the film's surfaces, thereby improving the PA performance, as shown in Figure 2.

2. Materials and methods

2.1 Preparation of thin films

The 100 nm thick ITO films coated on glass (1 $cm^2 \times 1.5$ cm^2) were used as a transparent conducting oxide substrate. The ITO glass substrates were cleaned under an ultrasonic process with acetone, methanol, and DI water, each for 15 min, respectively. After that, 1-layer films with 100 nm thick metallic Ti and W layers were deposited on the ITO glass substrate using DC magnetron sputtering and OAD at 85°, as shown in Figure 3(a). The 2-inch Ti disc (99.995% purity) and W disc (99.95% purity) (Kurt J. Lesker Company) were used as the targets. Argon (99.999% purity) at a flow rate of 15 sccm was used as the sputtering gas in a high vacuum chamber system. The system had a base pressure of 5.0×10^{-5} mbar, maintained by a rotary pump coupled with a diffusion pump, and an operating pressure of 2.5×10^{-2} mbar for all deposited films. Moreover, 2-layer films (ITO/Ti/W and ITO/W/Ti) were deposited with a total thickness of 100 nm, each layer being 50 nm thick. Finally, all films were oxidized by the TO in air at 500°C for 1 h within a furnace, as shown in Figure 3(b). These samples are summarized in Table 1. Photographs of the as-deposited Ti, W, Ti/W, and W/Ti films, and after the TO process at 500°C for 1 h, are shown in Figure 4.

2.2 Characterization of thin films

The top and cross-sectional views before and after the TO were observed by FE-SEM (Tescan Mira3, Czech Republic). Elemental composition was analyzed by EDS. Crystal structures were determined by XRD (D2 PHASER, Bruker) with Cu K_α radiation at 1.54 Å, scanning from 20° to 80° with a time per step of 0.2 s and increments of 0.02°. Transmittance (T%) in the range of 200 nm to 1000 nm was measured by UV-Vis spectrophotometer (Genesys S10, Thermo Scientific). Furthermore, the colored films were achieved through EC by applying a 2.0 V DC supply, connecting the films as the cathode, Pb as the anode, and immersing them in 0.1 M H_2SO_4 for 1 min.

After that, the PA performance of the films in the pre-color and colored states was tested by monitoring the relative absorbance of MB at 664 nm with a base concentration of 0.05 mM under UV irradiance (300 $\mu W \cdot cm^{-2}$, Silver light 10W/T8/BL Blacklight). Finally, the current density was measured by CV testing (Wuhan Corrtest Instruments Corp., Ltd.). A 3-electrode setup was used, with films serving as working electrodes, Ag/AgCl as reference electrodes, and Pt as counter electrodes. DC voltage ±2.0 V was applied at a constant scanning rate of 100 $mV \cdot s^{-1}$ in the H_2SO_4. Figure 5 illustrates the schematic setup for CV and PA testing.

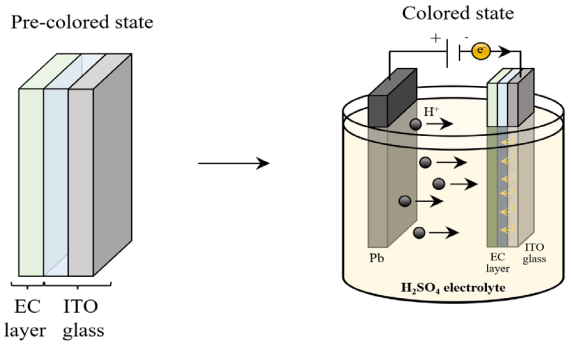

Figure 1. Schematic of EC process.

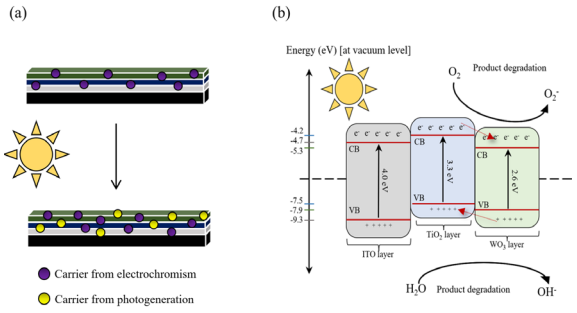

Figure 2. Mechanism of (a) carrier presence on the film surface in the colored state during irradiance light and (b) the PA of ITO/Ti/W films.

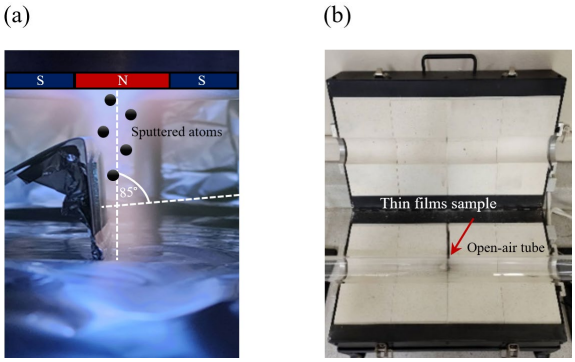

Figure 3. Schematic of experimental for (a) sputtering process with OAD, and (b) TO at 500°C for 1 h.

Table 1. Summary of preparation of ITO/Ti, ITO/W, ITO/Ti/W, and ITO/W/Ti films.

Samples	Sputtering power (Watts)		Total thickness (nm)	TO temperature and timen (°C, h)
	Ti	W		
ITO/Ti (TO)	100	-	100	500, 1
ITO/W (TO)	-	20	100	500, 1
ITO/Ti/W (TO)	100	20	50+50	500, 1
ITO/W/Ti (TO)	100	20	50+50	500, 1

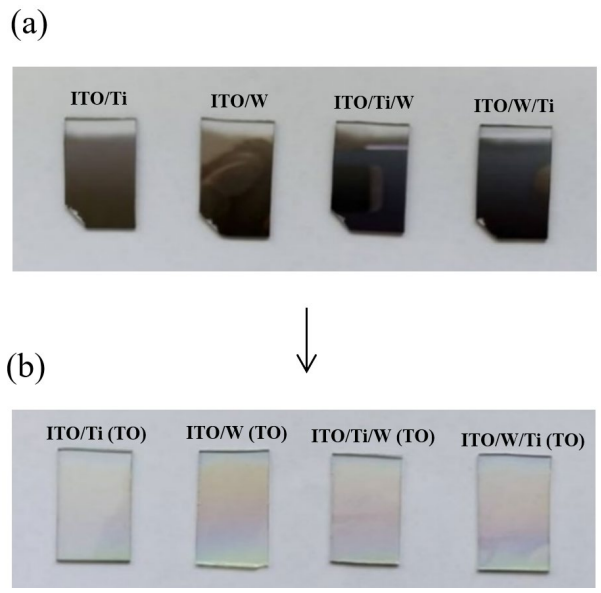

Figure 4. Photograph of (a) as-deposited metal Ti, W, Ti/W, and W/Ti films, and (b) after TO at 500°C for 1 h.

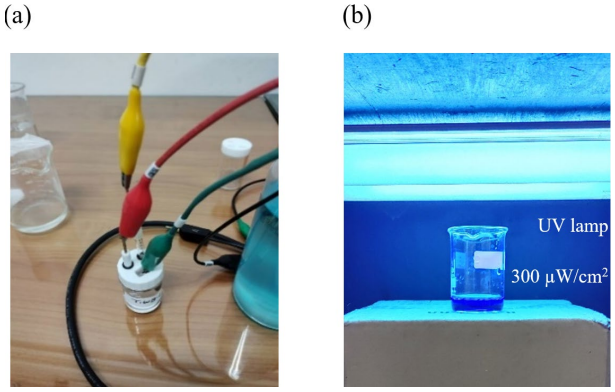

Figure 5. Experimental setup for (a) CV and (b) PA testing.

3. Results and discussion

3.1 Morphology and elemental composition

The top and cross-sectional views of the as-deposited and TO of ITO/Ti, ITO/W, ITO/Ti/W, and ITO/W/Ti are shown in Figure 6. The OAD techniques produce a nanorod structure according to the shadowing effect and the limitations of atom diffusion [28]. The realignment of nanorod alloys responds to the deposition rates (0.273 nm·s^{-1} and 0.115 nm·s^{-1} for Ti and W, respectively), with the higher deposition rate resulting in ITO/Ti showing orderly alloys. Conversely, ITO/W forms a porous structure, as observed in previous research [29], and the TO process results in the formation of oxides covering the surface.

The elemental compositions of as-deposited and after TO, represented by the weight percentages (wt%) from the EDS spectra, are shown in Figure 7 and Table 2 and Table 3. The Ti and W layers show a slightly different wt% of O due to the higher mass density of W atoms compared to Ti atoms, resulting in the EDS spectra being more likely to detect the presence of W atoms. In the 2-layer system, the wt% of Ti and W decreased by 50% due to the reduced thickness of the Ti and W layers. After TO, the wt% of O increased because the O atoms bonded with Ti and W atoms to form oxide components as described by the reactions: $Ti^{4+} + 2O^{2-} \rightarrow TiO_2$ and $W^{6+} + 3O^{2-} \rightarrow WO_3$.

In terms of elemental ratio, the 2-layer samples showed a slight difference in the Ti/W ratio. This can be attributed to the quantity of metal oxides in the samples. The porous surface of ITO/Ti/W allows O atoms to penetrate the film easily, leading to the strong formation of metal oxides, which is reflected in the reduced Ti and W wt%. On the other hand, the ITO/W/Ti sample has a more compact surface, resulting in a similar O wt% compared to ITO/Ti/W but higher Ti and W wt% [30]. Additionally, the other observed peaks correspond to components in the ITO glass (Si, In, Sn, Na, etc.).

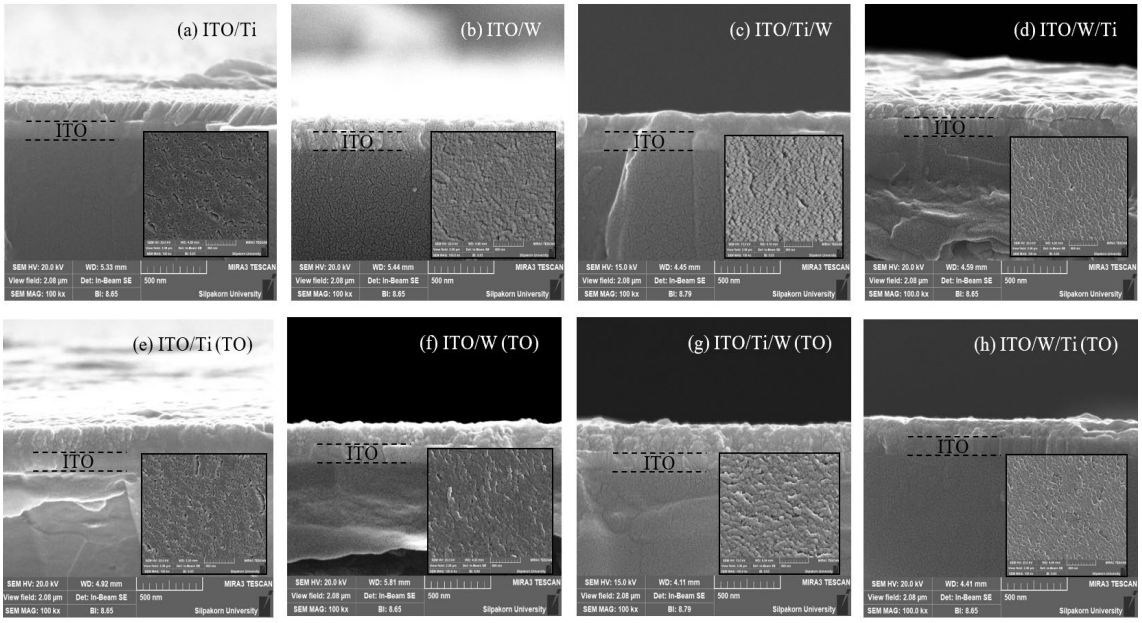

Figure 6. Top and cross-sectional views of FE-SEM images of as-deposited (a) Ti, (b) W, (c) Ti/W, and (d) W/Ti and after TO at 500°C for 1 h, (e) Ti, (f) W, (g) Ti/W, and (h) W/Ti.

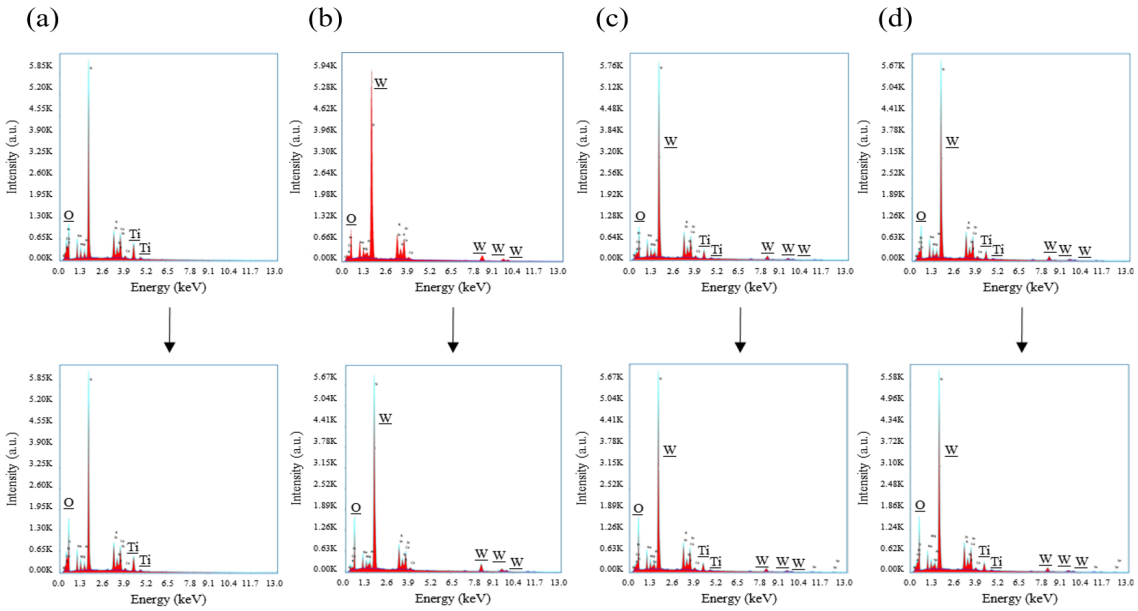

Figure 7. EDS spectra of (a) ITO/Ti, (b) ITO/W, (c) ITO/Ti/W, (d) ITO/W/Ti as-deposited (above) and after TO at 500°C for 1 h (below).

Table 2. Elemental composition of film samples as-deposited and after TO at 500°C for 1 h.

Samples	Elemental composition (wt%)					
	Ti		O		W	
	As-deposited	TO	As-deposited	TO	As-deposited	TO
ITO/Ti	7.63	6.34	23.77	30.46	-	-
ITO/W	-	-	12.99	24.62	28.86	25.24
ITO/Ti/W	4.02	3.21	19.02	26.31	14.67	11.94
ITO/W/Ti	3.82	3.22	19.40	26.40	15.54	13.05

Table 3. Elemental ratio of film samples as-deposited and after TO at 500°C for 1 h.

Samples	Elemental ratio					
	Ti/O		W/O		Ti/W	
	As-deposited	TO	As-deposited	TO	As-deposited	TO
ITO/Ti	0.32	0.21	-	-	-	-
ITO/W	-	-	2.22	1.03	-	-
ITO/Ti/W	0.21	0.12	0.77	0.45	0.27	0.27
ITO/W/Ti	0.20	0.12	0.80	0.49	0.25	0.25

3.2 Crystal structure

The crystal structures after TO at 500°C for 1 h were characterized by XRD, as shown in Figure 8. The small reflection at 2θ of 25.52° corresponded to the Miller indices (hkl) at the (101) plane of the TiO_2 anatase phase (JCPDS PDF no. 21-1272). The strong signals correspond to the primary reflections of WO_3 at 23.28°, 24.41°, 28.79°, 33.41°, 39.58°, and 41.67° corresponding to (002), (200), (112), (202), (210), and (222), respectively, with crystal orientations of the WO_3 orthorhombic phase (JCPDS PDF no. 83-0951).

In the case of the 2-layer samples (ITO/Ti/W and ITO/W/Ti) after TO, the anatase and orthorhombic phases were observed, similar to the 1-layer samples. This confirms that the crystal orientations did not change in the 2-layer system, regardless of whether the Ti or W layer was on top. However, the 2-layer samples showed evidence of lower peak intensity compared to the 1-layer samples because the ratio of the layers had decreased.

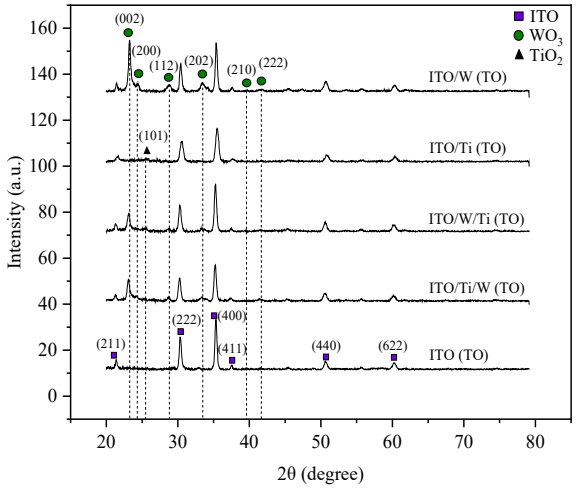

Figure 8. XRD patterns of the Ti and W sputtered with OAD 85° and after TO at 500°C for 1 h.

3.3 Optical properties

The optical transmittance spectra (T%) of the 1-layer and 2-layer film samples in the wavelength range of 200 nm to 1100 nm are shown in Figure 9 and used to determine the E_g values by Tauc's relation, as shown in Equation (1), where α is the absorption coefficient, hν is the incident photon energy, and E_g is the optical band gap energy.

$$\alpha h\nu = (h\nu - E_g)^n \quad (1)$$

where n = 2 for indirect transition of the E_g and intercepts of the tangent drawn at the absorption function to the energy axis at zero absorption are evaluated to get the E_g values.

After the TO, the film samples exhibited high transparency, and the E_g values were found to be 3.64, 3.67, 3.76, and 3.78 eV for ITO/Ti (TO), ITO/Ti/W (TO), ITO/W (TO), and ITO/W/Ti (TO), respectively. The results of the E_g values provide evidence of charge transfer between the Ti and W layers, especially in the W layer, where there is a change to the WO_3 orthorhombic phase. This phase change results in a reduced band alignment strategy in the 2-layer system [31,32].

3.4 Photocatalytic performance

In this study, the 1-layer and 2-layer films are divided into two states: i) pre-color state and ii) colored state. The colored state is achieved by applying a 2.0 V DC, connecting film as the cathode, and Pb as the anode, before immersion in H_2SO_4 as the electrolyte for 1 min, followed by the EC process.

The PA performance was evaluated through 4 iterations of tests by monitoring the degradation of 0.05 mM MB as an organic pollutant. The relative absorbance at 664 nm was measured and plotted against time to investigate the degradation over a total of 250 min. For the first 50 min, we observed the adsorption-desorption on the surface by sealing the samples in the dark. The remaining 200 min were conducted under UV irradiation at an intensity of 300 $\mu W \cdot cm^{-2}$ with recordings taken every 50 min. The chemical kinetics can be used to describe the behavior of the MB degradation rate, which follows a first-order reaction as described in Equation (2) [33].

$$\mathrm{Ln}\left(\frac{C}{C_0}\right) = kt \quad (2)$$

where C is the MB concentration, C_0 is the initial MB concentration (0.05 mM), k is the first-order rate constant, and t is time.

3.4.1 PA in the pre-color state

The first step of observation takes place in the pre-color state. The results are presented in Figure 10 and Figure 11. The first 50 min in darkness revealed absorption and fast activity by the catalyst surface. After the UV irradiation, the MB concentration clearly decreased due to the redox reaction. For the 1-layer samples, ITO/Ti (TO) showed a high photodegradation performance, benefiting from the catalytic properties of Ti compared to ITO/W (TO).

For the 2-layer films, the position of the layers significantly affected their PA performance. In the case of ITO/Ti/W (TO), the photodegradation performance was comparable to ITO/Ti (TO), despite the reduced thickness of the Ti layer. This indicates that the Ti layer plays the role of catalyst, and the W layer contributes to initial absorption [34,35], aiding the generation of e^--hole pairs and reducing the recombination rate due to e^- acceptance efficiency [36-39]. However, ITO/W/Ti (TO) did not perform effectively in photodegradation, showing a slower degradation rate because the ITO and Ti layers acted as barriers, obstructing the redox reaction by trapping e^- in the W layer [40], as shown in Figure 12.

Regarding durability, after cycling tests, ITO/Ti (TO) showed a decrease in performance, trending towards the performance of ITO/Ti/W (TO) after 4 tests of photodegradation under UV irradiation. Nonetheless, both ITO/Ti (TO) and ITO/Ti/W (TO) showed strong degradation performance and were chosen for photodegradation testing in the colored state.

3.4.2 PA in the colored state

After the first observation step, the 1-layer and 2-layer ITO/Ti and ITO/Ti/W samples were chosen based on their PA performance in the pre-color state. The next step of PA testing was conducted in the colored state by applying 2 V DC to the film, with the film as the cathode and Pb as the anode, and immersing it in H_2SO_4 for 1 min. The testing conditions were the same as in the pre-color state. Additionally, we studied the mechanism and stability of the film in the colored state during PA testing by measuring T% and calculating E_g before and after the EC process. We also collected T% at each step and observed photodegradation during the 1st test.

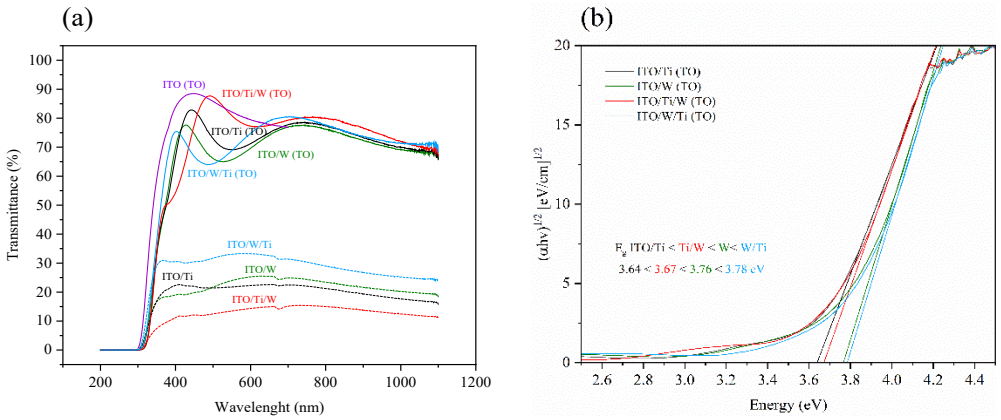

Figure 9. (a) T% and (b) E_g values from Tauc's plot of the film sample as-deposited and after TO at 500°C for 1 h.

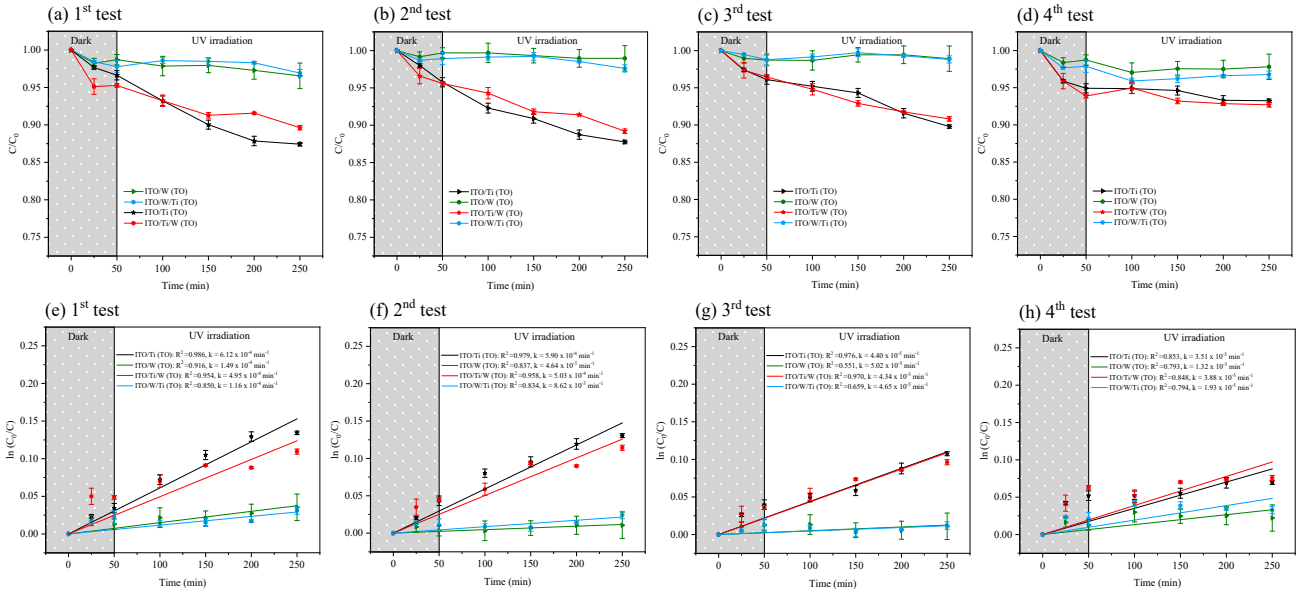

Figure 10. (a-d) Degradation of MB by measuring relative absorbance at 664 nm versus testing time and (e-h) the first-order rate constants for TO samples from 4 tests.

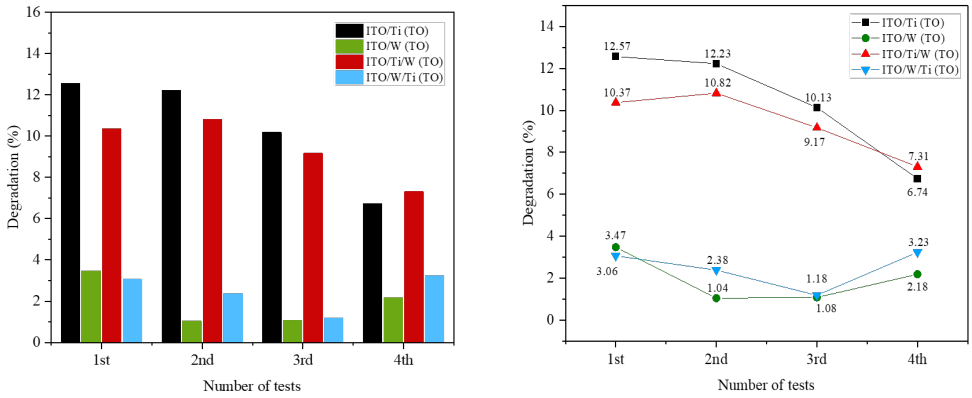

Figure 11. Comparison of the degradation % of thin films after TO at 500°C for 1 h based on data from 4 tests.

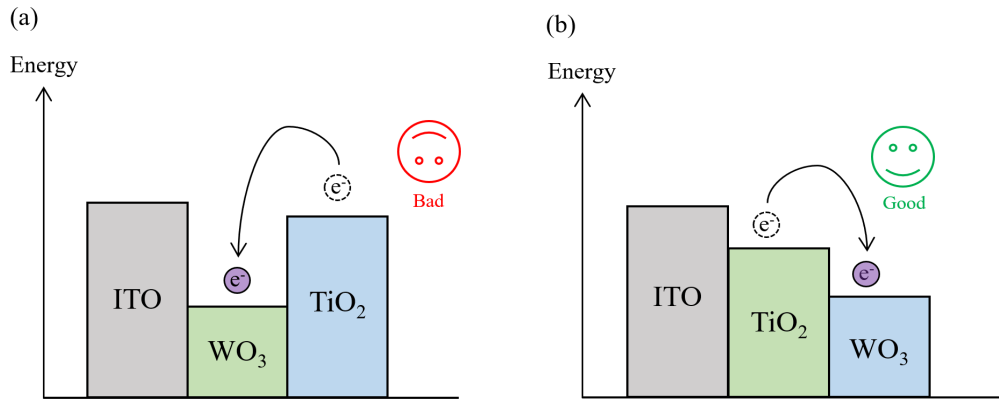

Figure 12. Effects of e^- transfer from layer arrangement of (a) ITO/W/Ti (TO), and (b) ITO/Ti/W (TO).

The results of T% and E_g of the films in both the pre-color and colored states are represented by dashed and solid lines, respectively, as shown in Figure 13. In the colored state, C-ITO/Ti (TO) exhibits only slight changes compared to C-ITO/Ti/W (TO), which shows significant absorption in the green spectrum and appears as a deep blue color. This is because the W layer, being a strong EC material, facilitates the quantity of ions and e^- into the structure, thereby enhancing the change in optical properties [41].

In terms of E_g, we found that for C-ITO/Ti/W (TO), right after the EC process, the E_g slightly increased to 3.71 eV and then decreased back to 3.77 eV as the film started bleaching after immersion in MB in a dark location for 25 min, and it was completely bleached after

100 min. In contrast, the C-ITO/Ti (TO) did not show a significant change in E_g and remained at 3.60 eV for 250 min. This behavior may be explained by the charge quantity and coloration efficiency in the EC effect.

The PA performance was observed using the same method as in the pre-color state, as shown in Figure 14 and summarized in Figure 15. After the EC process, the degradation of C-ITO/Ti/W (TO) increased from 12.78% to 15.46%, and C-ITO/Ti (TO) from 21.69% to 22.37%. This clearly demonstrates the effect of EC properties on increasing degradation efficiency, providing the evidence that the colored state does affect PA performance. The EC effect allows charge insertion and storage/trapping in the film's structure by forming specific compounds (H_xWO_x and H_xTiO_x), which induce absorption in specific spectra. We investigated the surface charge by monitoring the current density during the EC process using CV testing, as shown in Figure 16. The results show that C-ITO/Ti/W (TO) has a charge density of –0.0139 A·cm^{-2}, higher than C-ITO/Ti (TO) at –0.0112 A·cm^{-2}. This indicates that the films with more color formation had a greater number of carriers on the surface, leading to an increased oxidation-reduction rate of MB degradation [42-44].

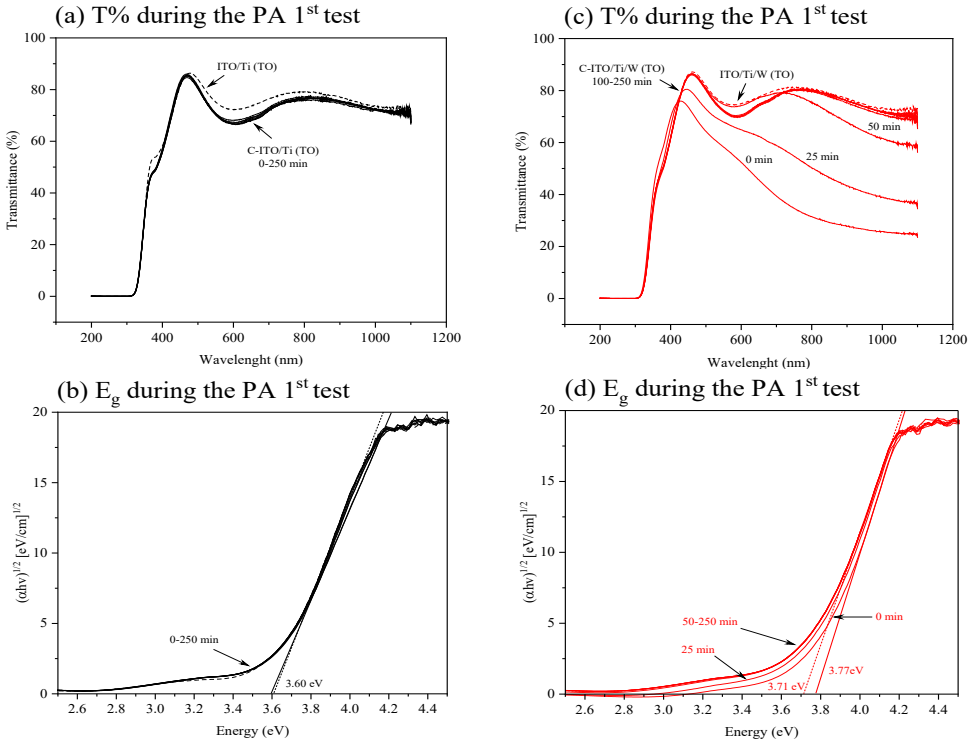

Figure 13. T% and before and after colored state and Tauc's plot relation of (a,b) ITO/Ti (c,d) and ITO/Ti/W during PA 1st test.

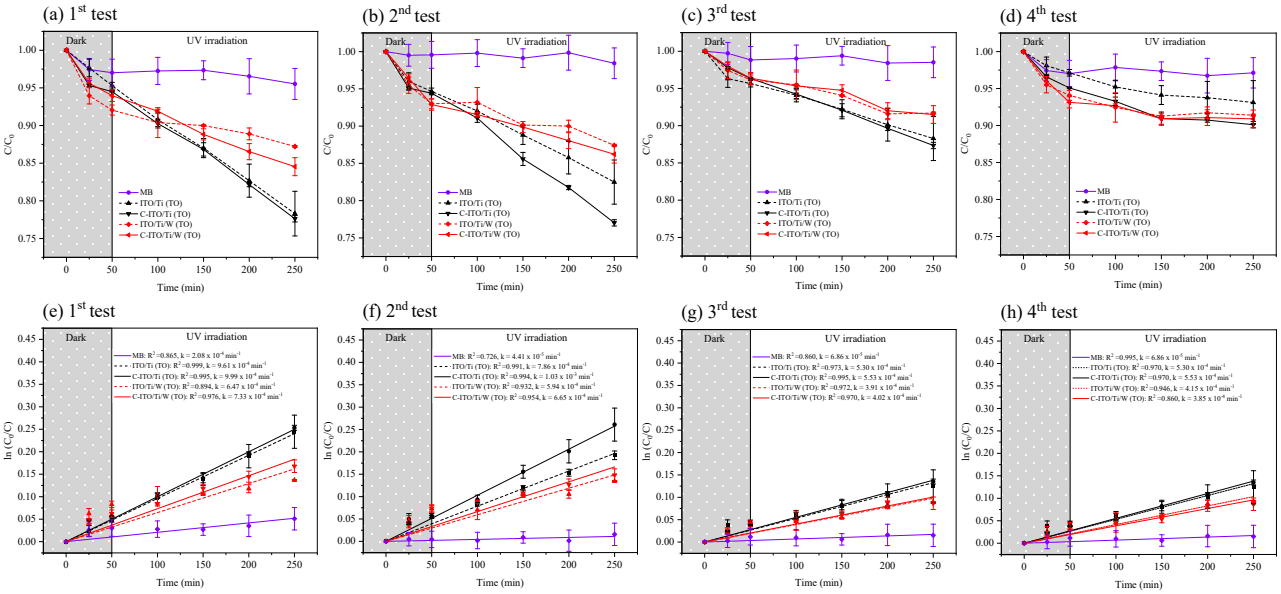

Figure 14. (a-d) Degradation of MB by measuring relative absorbance at 664 nm versus testing time and (e-h) the first-order rate constants for pre-color and colored states from 4 tests.

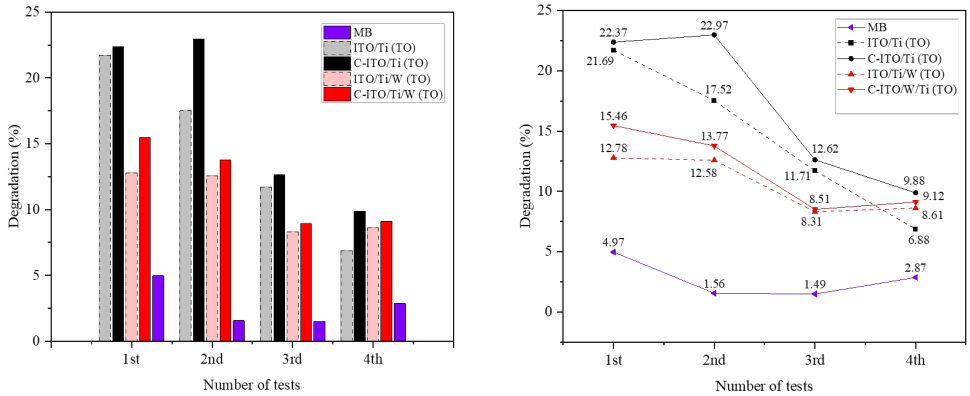

Figure 15. Comparison of the degradation % of pre-color and colored states for 1 h based on data from 4 tests.

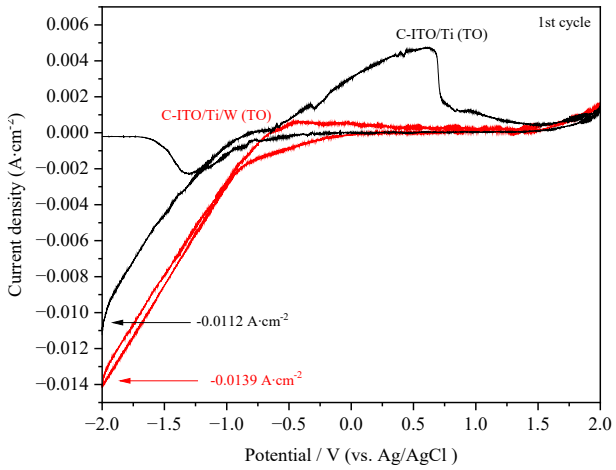

Figure 16. Cyclic voltammetry for the 1st cycle of C-ITO/Ti (TO) and C-ITO/Ti/W (TO).

Additionally, there are some interesting parts in C-ITO/Ti/W (TO) samples. Unfortunately, under our testing conditions, the colored state began to bleach after immersion in MB for 25 min, even without UV irradiation. We propose that if the colored state can be maintained long enough to be active in the UV region, the film may increase degradation by allowing activation in the visible spectrum.

4. Conclusions

The 1-layer and 2-layer Ti and W films were deposited using DC magnetron sputtering combined with an OAD technique, and the TO process was applied to form metal oxide films at 500°C for 1 h. The Ti layer exhibited an ordered tilted nanorod and the W layer exhibited a dense and porous surface due to the limitations of atom diffusion. XRD analysis revealed the crystalline structure of the anatase phase of TiO_2 and the orthorhombic phase of WO_3. The first step of observation of PA performance revealed that ITO/Ti (TO) and ITO/Ti/W (TO) exhibited higher degradation rates compared to ITO/W (TO) and ITO/W/Ti (TO), according to the charge transfer in band alignments of the heterojunction.

The ITO/Ti (TO) and ITO/Ti/W (TO) were chosen to test the PA performance in the colored state based on their degradation %, and the colored state achieved though the EC process revealed that C-ITO/Ti/W (TO) has higher coloration efficiency compared to C-ITO/Ti (TO) because the W layer plays a significant role as EC material which facilitates the charge into the structure confirmed by the current density in CV testing (–0.0139 and –0.0112 $A \cdot cm^{-2}$ for C-ITO/Ti/W (TO) and C-ITO/Ti (TO), respectively).

In terms of MB degradation under UV irradiance, both ITO/Ti and ITO/Ti/W in the colored state show higher degradation rates than in the pre-color state, and the degradation rate was enhanced by the double injection of e^- and ions by the EC effect.

Acknowledgment

This research is supported by Thailand Science Research and Innovation (TSRI) Fundamental Fund, fiscal year 2024. The authors would like to thank the Department of Physics, Faculty of Science and Technology, Thammasat University for providing the experimental facilities.

References

[1] N. T. Padmanabhan, N. Thomas, J. Louis, D. T. Mathew, P. Ganguly, H. John, S. C. Pillai, "Graphene coupled TiO_2 photocatalysts for environmental applications: A review," *Chemosphere*, vol. 271, p. 129506, 2021.

[2] F. Riboni, L. G. Bettini, D. W. Bahnemann, and E. Selli, "WO_3–TiO_2 vs. TiO_2 photocatalysts: effect of the W precursor and amount on the PA of mixed oxides," *Catalysis Today*, vol. 209, pp. 28-34, 2013.

[3] A. Karuppasamy, "Electrochromism and photocatalysis in dendrite structured Ti:WO_3 thin films grown by sputtering," *Applied Surface Science*, vol. 359, pp. 841-846, 2015.

[4] A. Hauch, A. Georg, U. O. Krašovec, and B. Orel, "Comparison of PhotoEC devices with different layer configurations," *Journal of The Electrochemical Society*, vol. 149, no. 9, pp. 159, 2002.

[5] W. Smith, A. Wolcott, R. C. Fitzmorris, J. Z. Zhang, and Y. Zhao, "Quasi-core-shell TiO_2/WO_3 and WO_3/TiO_2 nanorod arrays fabricated by glancing angle deposition for solar water splitting," *Journal of Materials Chemistry*, vol. 21, no. 29, p. 10792, 2011.

[6] Z. Dohčević-Mitrović, S. Stojadinović, and L. Lozzi, "WO_3/TiO_2 composite coatings: Structural, optical and photocatalytic properties," *Materials Research Bulletin*, vol. 83, pp. 217-224, 2016.

[7] N. Foad, and F. A. Bakar, "Synthesis of TiO_2 photocatalyst with tunable optical properties and exposed facet for textile wastewater treatment," *Results in Optics*, vol. 13, pp. 100545-100545, 2023.

[8] W. Promsuwan, P. Sujaridworakun, and W. Reainthippayasakul, "Synthesis of zinc oxide photocatalysts from zinc-dust waste for organic dye degradation," *Journal of metals, materials and minerals*, vol. 33, no. 2, pp. 58-64, 2023.

[9] C. Tangwongputti, P. Reubroycharoen, and P. Sujaridworakun, "Facile synthesis of heterostructured g-C_3N_4/Ag -TiO_2 photocatalysts with enhanced visible-light photocatalytic performance," *Journal of metals, materials and minerals*, vol. 32, no. 1, pp. 48-54, 2022.

[10] Y. Yao, D. Sang, L. Zou, Q. Wang, and C. Liu., "A review on the properties and applications of WO_3 nanostructure-based optical and electronic devices," , vol 11 no. 8, p. 2136, 2021.

[11] S. Park, Y. Quan, S. Kim, H. Kim, D. Chun, C. S. Lee, M. Taya, W. Chu, and S. Ahn, "A review on fabrication processes for EC devices," *International Journal of Precision Engineering and Manufacturing-Green Technology*, vol. 3, no. 4, pp. 397-421, 2016.

[12] Y. Ren, X. Zhou, Q. Wang, and G. Zhao, "Combined redox and plasmonic EC effects in WO_3/ITO double-layer films," *Journal of Sol-Gel Science and Technology*, vol. 85, no. 3, pp. 732-742, 2018.

[13] K. M. Karuppasamy, and A. Subrahmanyam, "The EC and photocatalytic properties of electron beam evaporated vanadium-doped tungsten oxide thin films," *Solar Energy Materials and Solar Cells*, vol. 92, no. 11, pp. 1322-1326, 2008.

[14] H. Zheng, J. Z. Ou, M. S. Strano, R. B. Kaner, A. Mitchell, and K. Kalantar-zadeh, "Nanostructured tungsten oxide-properties, synthesis, and applications," *Advanced Functional Materials*, vol. 21, no. 12, pp. 2175-2196, 2011.

[15] W. Li, P. Da, Y. Zhang, Y. Wang, X. Lin, X. Gong, and G. Zheng, "WO_3 nanoflakes for enhanced photoelectrochemical conversion," *ACS Nano*, vol. 8, no. 11, pp. 11770-11777, 2014.

[16] J. Yan, T. Wang, G. Wu, W. Dai, N. Guan, L. Li, and J. Gong, "Tungsten oxide single crystal nanosheets for enhanced multichannel solar light harvesting," *Advanced Materials*, vol. 27, no. 9, pp. 1580-1586, 2015.

[17] C. Salawan, M. Aiempanakit, K. Aiempanakit, C. Chananonnawathorn, P. Eiamchai, and M. Horprathum, "Effects of oblique angle deposition on optical and morphological properties of WO_3 nanorod films for EC application," *Materials Today: Proceedings*, vol. 4, no. 5, pp. 6423-6429, 2017.

[18] W. A. Smith, Z. Y. Zhang, and Y. Zhao, "Structural and optical characterization of WO_3 nanorods/films prepared by oblique angle deposition," *Journal of vacuum science & technology*, vol. 25, no. 6, pp. 1875-1881, 2007.

[19] Y. Liang, P. Wang, Y. Wang, Y. Dai, Z. Hu, D. E. Tranca, R. Hristu, S.G. Stanciu, A. Toma, G. A. Stanciu, X. Wang, and E. Fu, "Growth mechanisms and the effects of deposition parameters on the structure and properties of high entropy film by magnetron sputtering," *Materials*, vol. 12, no. 18, pp. 3008-3008, 2019.

[20] S. R. Damkale, S. S. Arbuj, G. Umarji, S. Rane, and B. B. Kale, "Highly crystalline anatase TiO_2 nanocuboids as an efficient photocatalyst for hydrogen generation," *RSC Advances*, vol. 11, no. 13, pp. 7587-7599, 2021.

[21] J. Yang, X. Zhang,H. Liu,C. Wang, S. Liu,P. Sun, L. Wang, and Y. Liu, "Heterostructured TiO_2/WO_3 porous microspheres: Preparation, characterization and photocatalytic properties," *Catalysis Today*, vol. 201, pp. 195-202, 2013.

[22] S. Higashimoto, T. Shishido, Y. Ohno, M. Azuma, M. Takahashi, and M. Anpo, "Photocharge-discharge behaviors of hybrid WO_3/TiO_2 Film Electrodes," *Journal of The Electrochemical Society*, vol. 154, no. 2, p. 48, 2007.

[23] S. Bogati, A. Georg, and W. Graf, "Photo EC devices based on sputtered WO_3 and TiO_2 films," *Solar Energy Materials and Solar Cells*, vol. 163, pp. 170-177, 2017.

[24] Z. Xia, H. Wang, Y. Su, P. Tang, M. Dai, H. Lin, Z. Zhang, and Q. Shi, "Enhanced EC properties by improvement of crystallinity for sputtered WO_3 film," *Coatings*, vol. 10, no. 6, pp. 577-577, 2020.

[25] M. H. Kim, H. W. Choi, and K. H. Kim, "Thickness dependence of WO_{3-x} thin films for EC device application," *Molecular Crystals and Liquid Crystals*, vol. 598, no. 1, pp. 54-61, 2014.

[26] G. F. Cai, D. Zhou, Q. Q. Xiong, J. H. Zhang, X. L. Wang, C. D. Gu, and J. P. Tu, "Efficient EC materials based on TiO_2 @WO_3 core/shell nanorod arrays," *Solar Energy Materials and Solar Cells*, vol. 117, pp. 231-238, 2013.

[27] M. A. Arvizu, C. A. Triana, B. Stefanov, C. G. Granqvist, and G. A. Niklasson, "Electrochromism in sputter-deposited W–Ti oxide films: Durability enhancement due to Ti," *Solar Energy Materials and Solar Cells*, vol. 125, pp. 184-189, 2014.

[28] A. Barranco, A. Borras, A. R. Gonzalez-Elipe, and A. Palmero, "Perspectives on oblique angle deposition of thin films: From fundamentals to devices," *Progress in Materials Science*, vol. 76, pp. 59-153, 2016.

[29] C. Aiempanakit, A. Chanachai, N. Kanchai, M. Aiempanaki, and K. Aiempanakit, "EC property of tungsten trioxide films prepared by DC magnetron sputtering with oblique angle deposition and thermal oxidation," *Journal of metals, materials and minerals*, vol. 31, no. 2, pp. 123-128, 2021.

[30] C. Aiempanaki and K. Aiempanakit, "Structural development and phase transformation behavior of thermally-oxidization Ti by sputtering power and OAD technique," *Materials Chemistry and Physics*, vol. 280, p. 125814, 2022.

[31] W. A. Smith, and Y. Zhao, "Enhanced PA by aligned WO_3/TiO_2 two-layer nanorod arrays," *The Journal of Physical Chemistry C*, vol. 112, no. 49, pp. 19635-19641, 2008.

[32] D. Nagy, T. Firkala, E. Drotár, Á. Szegedi, K. László, and I. M. Szilágyi, "Photocatalytic WO_3/TiO_2 nanowires: WO_3 polymorphs influencing the atomic layer deposition of TiO_2," *RSC Advances*, vol. 6, no. 98, pp. 95369-95377, 2016.

[33] K. Saitow, Y. Wang, and S. Takahashi, "Mechano-synthesized orange TiO_2 shows significant photocatalysis under visible light," *Scientific Reports*, vol. 8, no. 1, 2018.

[34] L. Zhang, H. Wang, J. Liu, Q. Zhang, and H. Yan, "Mesoporous WO_3/TiO_2 nanocomposites photocatalyst for rapid degradation of methylene blue in aqueous medium," *International Journal of Engineering*, vol. 32, no. 10, 2019.

[35] C. P. Sajan, A. Naik, and H. N. Girish, "Hydrothermal fabrication of WO_3-modified TiO_2 crystals and their efficiency in photocatalytic degradation of FCF," *International Journal of Environmental Science and Technology*, vol. 14, no. 7, pp. 1513-1524, 2017.

[36] E. Vasilaki, D. Vernardou, G. Kenanakis, M. Vamvakaki, and N. Katsarakis, "TiO_2/WO_3 photoactive bilayers in the UV-Vis light region," *Applied Physics A*, vol. 123, no. 4, 2017.

[37] K. Tennakone, O.A. Ileperuma, J. Bandara, and W.C.B. Kiridena, "TiO_2 and WO_3 semiconductor particles in contact: photochemical reduction of WO_3 to the non-stoichiometric blue form," *Semiconductor Science and Technology*, vol. 7, no. 3, pp. 423-424, 1992.

[38] C. Khare, K. Sliozberg, R. Meyer, A. Savan, W. Schuhmann, and A. Ludwig, "Layered WO_3/TiO_2 nanostructures with enhanced photocurrent densities," *International Journal of Hydrogen Energy*, vol. 38, no. 36, pp. 15954-15964, 2013.

[39] Y. C. Chen, T. Y. Lin, T. L. Chen, Y. D. Li, and K. W. Weng, "EC properties of tungsten-titanium oxide films," *Journal of Nano science and Nanotechnology*, vol. 12, no. 2, pp. 1296-1300, 2012.

[40] M. V. Dozzi, S. Marzorati, M. Longhi, M. Coduri, L. Artiglia, and E. Selli, "PA of TiO_2-WO_3 mixed oxides in relation to electron transfer efficiency," *Applied Catalysis B: Environmental*, vol. 186, pp. 157-165, 2016.

[41] C. Aiempanakit, R. Momkhunthod, and K. Aiempanakit, “Electrochromism in nanoporous tungsten trioxide films prepared through anodization and thermal oxidation,” *Integrated Ferroelectrics*, vol. 222:1, pp. 84-92, 2021.

[42] I. Alves, G. Byzynski, M. Dawson, and C. Ribeiro, "Charge transfer mechanism of WO_3/TiO_2 heterostructure for photoelectronchemical water splitting," *Journal of Photochemistry and Photobiology A: Chemistry*, vol. 339, pp. 95-102, 2017.

[43] L. Cao, J. Yuan, M. Chen, and W. Shangguan, "Photocatalytic energy storage ability of TiO_2-WO_3 composite prepared by wet-chemical technique," *Journal of Environmental Sciences*, vol. 22, no. 3, pp. 454-459, 2010.

[44] L. Zhang, J. Guo, B. Hao, and H. Ma, "WO_3/TiO_2 heterojunction photocatalyst prepared by reactive magnetron sputtering for Rhodamine B dye degradation," *Optical Materials*, vol. 133, p. 113035, 2022.